Reduced expression of PD-L1 and IDO1 characterises early response to antimonial therapy in cutaneous leishmaniasis patients.

Nidhi S. Dey[1‡], Sujai Senarathna[2‡], Vijani Somaratne[3], Nayani Madarasinghe[4], Bimalka Seneviratne[5], Luiza Campos Reis[6], Srija Moulik[7], Pegine Walrad[8], Mitali Chatterjee[7], Hiro Goto[6], Renu Wickremasinghe[2], Dimitris Lagos[1], Paul M. Kaye[1*] and Shalindra Ranasinghe[2*].

[1]York Biomedical Research Institute, Hull York Medical School, University of York, UK.

[2]Department of Parasitology, University of Sri Jayewardenepura, Sri Lanka.

[3]Dermatology Unit, District General Hospital Hambantota, Sri Lanka

[4]Dermatology Unit, Teaching Hospital Anuradhapura, Sri Lanka.

[5]Deparment of Pathology, University of Sri Jayewardenepura, Sri Lanka

[6]Instituto de Medicina Tropical de São Paulo, Faculdade de Medicina, Universidade de São Paulo, Brazil.

[7]Department of Pharmacology, Institute of Postgraduate Medical Education and Research, Kolkata, India.

[8]York Biomedical Research Institute, Dept. of Biology, University of York, UK.

[‡] NSD and SS contributed equally to this work.

*Correspondence: paul.kaye@york.ac.uk; ishalindra@sjp.ac.lk

Cutaneous leishmaniasis (CL) is a disfiguring disease caused by infection with *Leishmania* parasites and is characterised by parasitism of the dermis and chronic inflammation. Whilst T cell responses to *Leishmania* are essential for both parasite clearance and disease resolution they also drive inflammation, and clinical presentation reflects the balance of these opposing activities[1]. Pentavalent antimonials (e.g. sodium stibogluconate; SSG) remain the first line drugs for CL, even though treatment may be protracted and painful. Although evidence from animal models indicates that an effective clinical response to antimonials requires immune-drug synergy[2], little is known about how this operates in human disease. Here, we studied formalin fixed paraffin embedded (FFPE) skin biopsies from patients in Sri Lanka with CL, at presentation and during intra-lesional SSG treatment. Immune-targeted transcriptomics in a test patient cohort indicated heightened immune checkpoint pathway expression at presentation. We confirmed reduced PD-L1 and IDO1 protein expression on treatment in a second validation cohort, using digital spatial profiling and quantitative immunohistochemistry. PD-L1 and IDO1 expression on CD68^{+} monocytes / macrophages was positively correlated with the degree of intracellular parasitism, as determined by parasite-specific RNA FISH. Our data support a model whereby the initial anti-leishmanial activity of antimonial drugs alleviates checkpoint inhibition of T cell immunity, thus facilitating immune-drug synergism and clinical cure. We suggest a need to evaluate shorter course SSG treatment and/or the use of checkpoint inhibition as an adjunct host directed therapy (HDT) in CL.

One billion people are thought to be at risk of leishmaniasis, a group of diseases caused by infection with protozoan parasites of the genus *Leishmania* and transmitted by phlebotomine sand flies[3-5]. Approximately 600,000 – 1 million new cases of CL occur, with a broad global

50 distribution, often leading to stigma and reduced life chances and placing a burden on health
51 services[6,7]. Treatment options for CL have changed little in over 70 years, since pentavalent
52 antimonial drugs were first introduced, and there are scant new treatments on the horizon[8,9].
53 Sri Lanka is endemic for CL [10] with the first autochthonous case being reported in 1992[11].
54 Sri Lankan CL is caused by *Leishmania donovani* zymodeme MON-37[12-14], usually
55 associated with visceral leishmaniasis. Current treatment for CL in Sri Lanka involves
56 weekly intra-lesional or daily intra-muscular administration of SSG, with or without
57 cryotherapy, based on the site and size of the lesion and response to treatment. Cure often
58 takes many months, and some patients may fail to respond completely or withdraw from
59 treatment[15]. It is widely proposed that immune-drug synergy is required for fully effective
60 treatment in leishmaniasis and that host directed therapy (HDT) may have an important future
61 role in patient management [16,17,18], but few validated targets have emerged.
62
63 We reasoned that examination of the intra-lesional response early after the onset of therapy
64 might reveal potential mechanisms underpinning immune-drug synergy and / or targets for
65 HDT. We conducted a targeted transcriptomic analysis of the lesion site in a test cohort of 6
66 patients with typical homogeneous nodulo-ulcerative CL lesions (3 females, 3 males; mean
67 age ± standard deviation, 34.00 ± 11.05 years; (**Extended Data Fig. 1-3** and **Extended Data**
68 **Table 1**). Patients had 1-3 lesions with a mean time of diagnosis of 6.75 ± 5.8 months
69 (**Extended Data Table 1)** and received intra-lesional SSG weekly (0.5-2ml/cm^2). At
70 presentation, the amastigote density grading, based on slit skin smears (SSS) ranged from 0-6
71 (median =3) and was 0-3 after two weekly doses of SSG (median =2.5; **Extended Data**
72 **Table 1**). Based on amastigote detection in H&E stained biopsy sections, 5/6 patients
73 (**Extended Data Fig. 3**) showed improvement in amastigote grade[19] after two rounds of SSG.
74 One patient was lost to follow up (patient P1). 14.4 ± 4.15 doses of SSG were required to

75 reach clinical cure (defined as complete re-epithelialization and flattening of edges;
76 **Extended Data Table 1**) in the 5 patients followed to completion.
77
78 To define CL-associated immune gene expression signatures, RNA was extracted from FFPE
79 lesion biopsies at baseline and after 2 weeks of treatment (**Fig. 1a and Extended Data Table**
80 **1**) and analysed using a Nanostring PanCancer Immunology Panel 770 gene code set. We
81 compared the transcriptomic profile pre- and on-treatment (**Methods and Extended Data**
82 **Fig. 4**) and identified 120 transcripts that were significantly differentially expressed (DE)
83 (adjusted p-value<0.01; 105 downregulated, 15 upregulated; **Fig. 1a-d** and **Extended Data**
84 **Table 2**). Amongst the top 20 down regulated DE transcripts STRING[20] identified cell
85 migration (FDR= 6.33E-11; including interferon inducible chemokines like *CXCL9,*
86 *CXCL10, CXCL11*, *CCL19, CCL8)*) and regulators of immune response (FDR=8.55E-10;
87 including *IDO1, LAG3* and *CD274/PD-L1*) as highly enriched pathways (**Fig. 1c**).
88 Surprisingly, common effector and regulatory cytokines associated with human CL[1],
89 including *IFN-γ*, *IL-10*, *TNF*, *IL-7*, *IL-6*, *IL-4*, *TGFB1,* were not significantly different at this
90 early time point after the start of treatment (**Extended Data Table 3**). Transcripts of
91 inflammatory mediators like *CXCL10*, *GZMB*, *CCL2* and *CCR7* (receptor for CCL19),
92 previously shown to be associated with other forms of murine[21-23] and/or human CL[24-26] were
93 also found to be downregulated with initiation of treatment.
94
95 We next conducted multiplexed antibody digital spatial profiling[27] for 59 immune targets,
96 selecting regions of interest (ROIs) based on $CD3^+$ and/or $CD68^+$ expression (**Fig. 2**). A total
97 of 33 ROIs were analysed from three patients (P4, P6 and P7) at presentation and on-
98 treatment (**Extended Data Fig. 5** and **Fig. 2a-f**), confirming that IDO1 and PD-L1 were
99 selectively reduced in expression upon treatment (**Fig. 2g-h, j**). Other immune checkpoints

100 (LAG3, CTLA4, OX40/TNFRSF4) and immune regulators (e.g. TGFB1, FOXP3) showed no
101 change on-treatment (**Fig 2g, i**).
102
103 Next, we sought to validate these findings by evaluating IDO1 and PD-L1 expression in an
104 independent validation cohort of 25 CL patients (5 females, 20 males; mean age ± standard
105 deviation, 44.12 ± 11.25 years; time to diagnosis 6.76 ± 8.2 months; **Extended Data Fig. 6**
106 **and 7** and **Extended Data Table 4**). Using an accepted cut-off of >5% of cells being
107 positive[28], 24/25 of the patients expressed IDO1 (Histochemical (H)-score [29] median = 97.5;
108 range 0.40 - 168) and 23/25 of patients had a reduction in the abundance of $IDO1^+$ cells on
109 treatment (H-score median = 17.8; range 0.05 – 181; $p<0.001$; **Fig. 2k**). All patients were
110 PD-L1 positive at presentation (**Fig. 2l**; H-score median = 133.6; range 53.6-196.8) and 20/25
111 patients exhibited a reduction in the number of PD-L1 expressing cells on treatment (**Fig. 2l**;
112 H-score median = 78.1; range 3.5-145.3; $p <0.0001$). Collectively, these data indicate that
113 IDO1 and PD-L1 are highly expressed in the lesions of Sri Lankan CL patients and that
114 reduction in expression of these two checkpoint pathways represents an early response to
115 SSG.
116
117 Although *in vitro* studies had indicated that intracellular parasitism by *Leishmania* parasites
118 could affect the expression of PD-L1[30] and IDO1[31], this has not been validated in human
119 disease. To address this we combined IHC with RNA-FISH [32] for *Amastin* transcripts (as a
120 surrogate for viable amastigotes) and developed a StrataQuest image analysis pipeline
121 (**Extended Data Fig. 8a-f**). IDO1 was extensively co-localised with $CD68^+$ cells (**Fig. 3a**),
122 though $CD68^-$ $IDO1^+$ cells were also observed (**Fig. 3a and Extended Data Fig. 9a-b**).
123 Intracellular amastigotes were detected in both $IDO1^+CD68^+$ and $IDO1^-CD68^+$ cells (**Fig. 3a;**
124 **Extended Data Fig. 9a**). We binned the *Amastin*$^+$ $IDO1^+$ and *Amastin*$^-$ $IDO1^+$ cells based on

125 IDO1 mean fluorescent intensity (**Fig. 3b-d**; for gating strategy, see **Methods** and **Extended**
126 **Data Fig. 8a-f**). In all three patients studied (that showed positive *Amastin* expression;
127 **Methods**; **Extended Data Table 1**), we found that cells with abundant *Amastin* transcripts
128 expressed more IDO1^{+} than those with fewer or no *Amastin* transcripts (**Fig. 3b-f** and
129 **Extended Data Fig. 8g-l**).
130
131 Similarly, in 7 patients studied from a validation cohort that were *Amastin*$^{+}$ at presentation
132 (**Methods, Extended Data Table 5**), PD-L1 expression co-localised with CD68^{+}
133 macrophages (**Fig. 4a, Extended Data Fig. 9c**) and parasitized cells were both PD-L1^{+} and
134 PD-L1^{-} (**Fig. 4a**). Using a similar gating strategy (**Extended Data Fig. 10a-f**), we found that
135 cells containing abundant *Amastin* transcripts expressed more PD-L1 than cells with less or
136 no *Amastin* transcripts **(Fig. 4b-f, Extended Data Fig. 10g-l** and **Extended Data Fig. 11**).
137 These data show that, although a notable population of uninfected CD68^{+} cells contributes to
138 PD-L1 and IDO-1 expression within the CL lesion, intracellular parasitism leads to
139 heightened expression of checkpoint molecules by lesional monocytes and macrophages.
140
141 Both IDO1 and PD-L1 are important determinants of T cell activation and tolerance [33], with
142 well-defined mechanisms of action [34, 35] and both IDO1 [36, 34]and PD-L1 [28, 37, 38, 39, 40,41] have
143 well-established therapeutic pipelines. Furthermore, there is already strong pre-clinical
144 evidence supporting both an inhibitory role of these checkpoint pathways in various forms of
145 leishmaniasis and that checkpoint inhibition leads to accelerated cure [42,43, 44, 45] . The
146 elevated expression of negative immune regulators on infected macrophages, as shown here,
147 extends our understanding of how *Leishmania* parasites influence the function of their host
148 cell[46], with clear parallels to tumour associated macrophages[47]. More importantly, our
149 demonstration that a rapid reduction of expression of IDO1 and PD-L1 occurs early after the

150 onset of SSG treatment in human CL, has important clinical implications. First, it suggests a
151 model for drug-immune synergy, whereby early rounds of SSG treatment reduce intracellular
152 parasite burden and as a consequence there is reduced expression of the checkpoint molecules
153 IDO1 and PD-L1 and re-engagement of T cell effector function (**Extended Data Fig. 12**).
154 Importantly, this model suggests that continuation of SSG treatment until clinical cure is
155 achieved may be unnecessary. Second, adjunct HDT targeting these checkpoint pathways
156 may accelerate such changes in the lesional microenvironment and help minimise drug
157 dosage and treatment duration. With patients facing up to several months of intralesional
158 SSG treatment, there appears a compelling case to evaluate these hypotheses in future clinical
159 trials.
160

161 **Methods**

162 **Patients and patient derived samples:**

163 *Ethics statement*

164 The study was conducted in accords with the principles of the Declaration of Helsinki and
165 was approved by the Ethical Review Committee of the Faculty of Medical Sciences,
166 University of Jayewardenepura (Ref: 780/13 & 52/17) and the Department of Biology,
167 University of York. Two study groups were included in the study consisting of 6 patients
168 (pilot study) and 25 patients (validation study) aged 18 to 62 years who were willing and had
169 given written informed consent, and who had fulfilled the entry criteria. Patients were
170 enrolled from the Dermatology Unit, Teaching Hospital, Anuradhapura (THA) (Pilot study),
171 and District Base Hospital Embilipitiya (validation study), Sri Lanka. Exclusion criteria were
172 patients with travel history to a leishmaniasis endemic country, immunosuppression, diabetes
173 mellitus, HIV, chronic fever with hepatosplenomegaly, infected CL lesions, iatrogenic
174 infections following sample collection or chemotherapy and children below the age of 18. All

175 patients were physically examined by a dermatologist at every visit to exclude or treat
176 infected CL lesions, iatrogenic infections following sample collection or drug therapy.
177
178 *Test cohort*
179 All participants except one (P1; not contactable) completed the treatment course. All patients
180 were assessed on basis of SSS/ histopathology and/or clinical evaluation. In case of poor
181 correlation between SSS and histopathology, judgement was based on clinical assessment, as
182 it has been previously shown to be >90% accurate for diagnosis[48]. P4 was included as it fit
183 the clinical criteria for CL despite having no discernible amastigotes present[49].
184 All patients received weekly (0.5-2ml/cm2) intra-lesional SSG (including at the time of
185 sample collection), while 3/6 of patients also received adjunct cryotherapy at a later stage of
186 treatment when they were not responding sufficiently to intralesional SSG.
187
188 *Validation cohort*
189 Lesions were either papular (n=2), nodular (n=3), plaque (n=6) or ulcerated (dry n=12; wet
190 n=2) with mean ulcerated area of 51.13 mm^2 (± SD, 81.1) and area of induration ranging up
191 to 8000 mm^2 (mean ± SD, 1430.2 ± 1966.9). In addition to clinical assessment, CL was
192 diagnosed by slit skin smears (SSS) (18/25) and PCR (25/25). Punch biopsies were taken
193 from these patients at baseline and after 4 weeks of treatment with weekly dose of 1 ml/cm^2
194 intralesional SSG. 24/25 patients cured within 6 months of the start of treatment.
195
196 *Slit skin smears (SSS):* Tissue scrapings from a 3mm superficial nick from the active edge of
197 the lesions were used to prepare smears on slides, stained with Giemsa and examined under
198 oil immersion microscopy for the presence of amastigotes. Parasite density was graded from
199 0 to 6+ according to WHO guidelines for VL[19]: 0—no parasites per 1000 high power fields

200 (HPF: x 1000 magnification); 1+: 1–10 parasites per 1000 HPFs; 2+: 1–10 parasites per 100
201 HPFs; 3+: 1–10 parasites per 10 HPFs; 4+: 1–10 parasites per HPF; 5+: 10–100 parasites per
202 HPF; and 6+: > 100 parasites per HPF.
203
204 *Punch Biopsy:* A 3mm diameter full thickness punch biopsy was taken from the edge of the
205 lesion under local anaesthesia, transported in formol saline and then fixed in paraffin blocks
206 and used for H&E and IF studies.
207 *PCR:*
208 From each lesion, another 2 mm diameter full thickness punch biopsy sample was taken from
209 the active edge, stored in RNA later at -20˚C and was subjected to DNA extraction using
210 QIAGEN DNeasy Blood & Tissue Kit. A volume of 2µl of this extracted DNA was
211 amplified with 100 pmols of previously described[50] set of primers LITSR/L5.8S that
212 amplifies a 320 bp fragment of ITS1 region of Leishmania genus-specific DNA in the
213 presence of 1.5 mM MgCl2, 25 mM Tris-HCL (pH 9.0), 25 mM NaCl, 200 µM each
214 deoxynucleotide triphosphate, 50 units/ml Taq DNA polymerase (Promega) in a final volume
215 of 10 µL. The PCR amplification cycles consisted of an initial denaturation at 95°C for 2
216 min, followed by 34 cycles of denaturation at 95°C for 20 s, annealing at 53°C for 30 s, and
217 extension at 72°C for 1 min, with a final extension of 72°C for 6 min[50,51]. Extracted DNA
218 from a pure culture was the positive control and no DNA sample was the negative control. A
219 volume of 5 µL from the PCR product was run at 100 V for 45 min on a 1.75% (w/v) wide
220 range agarose gel stained with 0.2 µg/mL ethidium bromide (EtBr) in 1X tris-acetate-EDTA
221 buffer. The image was visualised under UV light and captured by a computerised gel
222 documentation unit (Quantum ST5; Vilber Lourmat, Germany).
223 LITSR (forward): 5'-CTGGATCATTTTCCGATG-3' L 5.8S (reverse): 5'-
224 TGATACCACTTATCGCACTT-3'

225

226 **RNA isolation**

227 The total RNA was extracted from formalin-fixed paraffin-embedded (FFPE) patient samples
228 using RNeasy FFPE Kit (Qiagen) as per manufacturer's protocol. Briefly, 2 10μm sections
229 were cut from each block and put into deparaffinization buffer (Qiagen). Sample lysis was
230 done with Proteinase K digestion for 15 minutes. After lysis, samples were incubated at 80ºC
231 for 15 minutes followed by 15 minutes of DNase treatment. Finally, concentrated RNA was
232 purified using RNeasy MinElute spin columns, and eluted in a volume of 14–30 μl.

233

234 **NanoString nCounter assay**

235 RNA quality and size of RNA fragments for nanostring assay was assessed using the Agilent
236 2100 Bioanalyser at Technology Facility, University of York. One-hundred nanograms of
237 RNA was used for the analysis using the nCounter PanCancer Immune Profiling Panel (XT-
238 CSOMIP1-12, NanoString Technologies[52]). Processing of samples and data collection were
239 done at Centre for Genomic Research, University of Liverpool. Data analysis was performed
240 using the nSolver Advanced Analysis Software (NanoString Technologies) v2.0. Filtering of
241 samples using quality control criteria was performed and data was normalized by scaling with
242 the geometric mean of the built-in control gene probes for each sample according to the
243 manufacturer's recommendations.

244

245 **Bioinformatics analysis of the NanoString nCounter assay**

246 Log2-transformed normalised data was used to plot volcano plot of differentially expressed
247 genes in R using graphics package. Volcano Plot filtering (fold change ≥1.3, $P<0.05$) was
248 used to identify differentially expressed genes with statistical significance between the two
249 groups. Pair-wise correlation was calculated using Pearson's coefficients in R using stats

250 package to compare log2-transformed normalised data sets acquired from nsolver software
251 and then plotted in GraphPad. Student's t test was applied to compare normalized expression
252 values between groups. Physical and functional interactions between proteins were
253 determined using the STRING platform at a medium confidence score of 0.4.
254
255 **Nanostring DSP**
256 4μm thick sections were used for DSP analysis of 59 immune parameters (**Fig. 2g**) through
257 Nanostring Technology Access Program (TAP) on FFPE skin biopsies. Slides were stained
258 with CD3 and CD68 as morphological markers and with 62 oligo-nucleotide conjugated
259 antibodies on three patients P4, P6, P7 at presentation and on treatment. Amongst 12 ROIs
260 per sample, 11 ROIs were created and distributed uniformly on CD68+ macrophage and CD3
261 rich T cell areas and one was created outside the tissue on glass. Data were normalised to
262 geomean of area of all ROIs and to spike in controls. Glass values were deducted and data
263 distribution was normalised by taking log2 of the counts. Data was plotted from all 33 ROIs
264 on pre- and on-treatment sections and two-tailed unpaired Student's t test was performed to
265 calculate significance score**.**
266
267 **IF and FISH**
268 4 μm sections from FFPE blocks of skin biopsies were used for all analyses. Skin sections
269 were stained with H&E (Sigma Aldrich) and were imaged using Zeiss AxioScan.Z1 slide
270 scanner. For immunofluorescence and RNAScope FISH assay, paraffin was removed from
271 the formalin-fixed sections using Histo-clear followed by washes in alcohol and water.
272 Antigens were unmasked by mild boiling in RNAscope® Target Retrieval Reagent (15
273 minutes), peroxidase treatment followed by treatment with RNAscope® Protease Plus
274 Reagent for 30 minutes at 40^0C. Parasites were detected by FISH using a 13ZZ probe against

275 *L.Infantum*-amastin targeting 2-635 of LinJ.34.1010 (having 85% sequence homology with
276 LmjF.34.0500) for 2 hours at 40^0C and developed using manufacturer's protocol. For IF-
277 FISH dual staining, FISH was done first, followed by IF.
278
279 For IF, following a few washes with TBST (0.05% TBS Tween20), blocking was done with
280 5% (v/v) normal donkey serum, 5% (v/v) normal goat serum and 5% BSA (w/v) for 1 hr at
281 RT. Sections were then probed with, mouse anti-human CD3 (1:10, Abcam USA, ab17143),
282 rabbit anti-IDO1 (1:80, Cell Signaling Tech., D5J4E); rabbit anti-PD-L1 (1:150, Cell
283 Signaling Tech., E1L3N), rabbit anti-human CD68 (1:800, Abcam USA, ab213363), mouse
284 anti-human CD68 (1:100, Abcam USA, ab955), rabbit IgG isotype control (concentration
285 same as the primary, Abcam USA, ab172730, mouse IgG1 isotype control (BioLegend USA,
286 401401) overnight at 4^0C. Primary antibodies were detected by goat anti-mouse IgG (H+L)
287 cross-adsorbed secondary antibody, Alexa Fluor 488 (Thermo Fisher Scientific, USA, and
288 A11001) and goat anti-rabbit IgG (H+L) highly cross-adsorbed secondary antibody, Alexa
289 Fluor 555 (Thermo Fisher Scientific, USA, A21429). Sections were counterstained with
290 DAPI and mounted in Fluoroshield™ histology mounting medium.
291
292 **Image acquisition and analysis.**
293 Images were acquired using Zeiss AxioScan.Z1 slide scanner, Zeiss LSM 880 with Airyscan
294 on an Axio Observer.Z1 invert and Zeiss LSM 710 on an AxioImager. M2. Identical
295 exposure times and threshold settings were used for each channel on all sections of similar
296 experiments.
297 Quantification of IDO1, PD-L1, CD3 *Amastin*, and CD68 was performed using StrataQuest
298 Analysis Software (TissueGnostics). In brief, for IDO1, CD68 and PD-L1 cells, the software
299 segmented nuclei on the basis of the signal from the DAPI channel, then built and expanded a

300 mask over staining of IDO-1/ PD-L1. A cut off was applied on IDO-1/PDL-1 mean
301 intensities based on visual inspection of the tissue to delineate IDO1/ PD-L1 $^{+/-}$ cells. On the
302 IDO1 generated mask, algorithm searched for colocalization of a similar mask for CD68
303 signal for IDO1 CD68 double positive cells as well as IDO1^{+}CD68^{-} cells.
304 A separate layer was created to extract the information of *Amastin* positive dots in all
305 patients. *Amastin*$^{+}$ dots were detected in 3/6 (test cohort) and 7/25 (validation cohort) of
306 patients (within the limits of detection in thin sections; 4μ). Number of *Amastin* dots in
307 IDO1^{+} and PD-L1^{+} cells were computed and plotted in histograms (**Extended data Fig. 8f**
308 and **Extended Data Fig. 10f**). A cut-off of one was applied to number of *Amastin* dots to
309 look at IDO1^{+}*Amastin*$^{+}$/ PD-L1^{+}*Amastin*$^{+}$ nuclei. More histograms were plotted for PD-L1
310 and IDO1 mean intensity but gated onto the right and left quadrant of histograms for *Amastin*
311 dots to get information of parasite positive and negative cells, respectively (**Fig. 3c-d, 4c-d,**
312 **Extended Data Fig. 8f g-l, Extended Data Fig. 11**). Gates were then generated on
313 histograms of IDO1 and PD-L1 mean intensities to look at low, medium and highly labelled
314 cells and were coloured as cyan, red and orange/green, respectively in separate scattergrams
315 for *Amastin*$^{+}$/*Amastin*$^{-}$ PD-L1 and *Amastin*$^{+}$/*Amastin*$^{-}$ IDO1 cells.
316 Histochemical score (H-score[29]) was used to assay expression levels of IDO1 and PD-L1. H-
317 score was calculated on the basis of the formula = 0 x (% of IDO1/PD-L1^{-}) + 1 X (% of
318 weakly labelled IDO1/PD-L1^{+}) + 2 X (% of moderately labelled IDO1/PD-L1^{+}) + 3 X (% of
319 strongly labelled cells). Positive expression of PD-L1 and IDO1 was defined by positive
320 staining in >5% of cells[28].
321
322 **Statistics**

Statistical analysis was performed in GraphPad Prism (version 8) using paired and unpaired 2-tailed Student's t test, as indicated in the legends. A P value less than 0.05 (*) was considered significant.

Acknowledgments

The authors thank Dr. Pushpa Ilanngasinghe, histopathologist at University of Sri Jayewardenepura, Sri Lanka, staff at BioSciences Technology Facility Imaging and Cytometry Laboratory for assistance with Strataquest and confocal analysis, technical support at Nanostring Technologies for DSP data acquisition, TissueGnostics for assistance with Strataquest, Centre for Genomic Research, University of Liverpool for processing samples for Nanostring transcriptomics and all members of the laboratory for their useful comments and suggestions.

This work was supported by funding from the UK Medical Research Council / UK Aid Global Challenges Research Fund (MR/P024661/1 to PMK, SR, HG and MC) and Wellcome Trust Senior Investigator Award (WT104726 to PMK). The funders had no role in the design or conduct of the study of the decision to publish.

Author Contributions

NSD design, experimental data analysis writing ms

SS design, experimental, data analysis

VS experimental

NM experimental

BS experimental

LR experimental

SM experimental

PW, conceptualisation design, funding

MC, HG, conceptualisation, design, funding

RW conceptualisation, design of study

DL conceptualisation design, data analysis, funding

PMK[1] conceptualisation design, data analysis, funding, supervision

SR conceptualisation design, experimental, data analysis, funding, supervision

Competing Interests statement

Authors declare no conflict of interests.

Data availability statement

Source data for **Fig. 1a** is in **Extended Data Table 2. Extended Data Table 3** shows Log2 (fold change) and adjusted p-value of DE transcripts of common regulators/effectors of human leishmaniasis analysed in this study. Rest of the data that support the findings of this study are available from the corresponding author upon reasonable request. Digital Whole Slide Image files will be made available at https://leishpathnet.org.

364 **References**

365

366 1. Scott, P. & Novais, F.O. Cutaneous leishmaniasis: immune responses in protection and
367 pathogenesis. *Nat Rev Immunol* **16**, 581-592 (2016).
368 2. Murray, H.W., Oca, M.J., Granger, A.M. & Schreiber, R.D. Requirement for T cells and effect
369 of lymphokines in successful chemotherapy for an intracellular infection. Experimental
370 visceral leishmaniasis. *J Clin Invest* **83**, 1253-1257 (1989).
371 3. World Health Organization. Leishmaniasis. (2019, March 14).
372 4. Alvar, J.*, et al.* Leishmaniasis worldwide and global estimates of its incidence. *PLoS One* **7**,
373 e35671 (2012).
374 5. Drugs for Neglected Diseases initiative. About leishmaniasis. (2019,).
375 6. Alvar, J., Yactayo, S. & Bern, C. Leishmaniasis and poverty. *Trends Parasitol* **22**, 552-557
376 (2006).
377 7. Pires, M., Wright, B., Kaye, P.M., da Conceicao, V. & Churchill, R.C. The impact of
378 leishmaniasis on mental health and psychosocial well-being: A systematic review. *PLoS One*
379 **14**, e0223313 (2019).
380 8. de Menezes, J.P., Guedes, C.E., Petersen, A.L., Fraga, D.B. & Veras, P.S. Advances in
381 Development of New Treatment for Leishmaniasis. *Biomed Res Int* **2015**, 815023 (2015).
382 9. Singh, K., Garg, G. & Ali, V. Current Therapeutics, Their Problems and Thiol Metabolism as
383 Potential Drug Targets in Leishmaniasis. *Curr Drug Metab* **17**, 897-919 (2016).
384 10. World Health, O. Leishmaniasis country profile – priority countries. (2019).
385 11. Athukorale, D.N., Seneviratne, J.K., Ihalamulla, R.L. & Premaratne, U.N. Locally acquired
386 cutaneous leishmaniasis in Sri Lanka. *J Trop Med Hyg* **95**, 432-433 (1992).
387 12. Karunaweera, N.D., Pratlong, F., Siriwardane, H.V., Ihalamulla, R.L. & Dedet, J.P. Sri Lankan
388 cutaneous leishmaniasis is caused by Leishmania donovani zymodeme MON-37. *Trans R Soc*
389 *Trop Med Hyg* **97**, 380-381 (2003).
390 13. Ranasinghe, S.*, et al.* Leishmania donovani zymodeme MON-37 isolated from an
391 autochthonous visceral leishmaniasis patient in Sri Lanka. *Pathog Glob Health* **106**, 421-424
392 (2012).
393 14. Zhang, W.W.*, et al.* Genetic analysis of Leishmania donovani tropism using a naturally
394 attenuated cutaneous strain. *PLoS Pathog* **10**, e1004244 (2014).
395 15. Refai, F.W., Madarasingha, N.P., Fernandopulle, R. & Karunaweera, N. Nonresponsiveness to
396 standard treatment in cutaneous leishmaniasis: A case series from Sri Lanka. *Trop Parasitol*
397 **6**, 155-158 (2016).
398 16. Dalton, J.E. & Kaye, P.M. Immunomodulators: use in combined therapy against
399 leishmaniasis. *Expert Rev Anti Infect Ther* **8**, 739-742 (2010).
400 17. Sbaraglini, M.L.*, et al.* Neglected Tropical Protozoan Diseases: Drug Repositioning as a
401 Rational Option. *Curr Top Med Chem* **16**, 2201-2222 (2016).
402 18. Rao, S.P.S.*, et al.* Drug Discovery for Kinetoplastid Diseases: Future Directions. *ACS Infect Dis*
403 **5**, 152-157 (2019).
404 19. WHO Expert Committee on the Control of the Leishmaniases and World Health Organization.
405 Control of the leishmaniases: report of a meeting of the WHO Expert Commitee on the
406 Control of Leishmaniases, Geneva, 22-26 March 2010. (World Health Organization, Geneva,
407 2010).
408 20. Szklarczyk, D.*, et al.* STRING v11: protein-protein association networks with increased
409 coverage, supporting functional discovery in genome-wide experimental datasets. *Nucleic*
410 *Acids Res* **47**, D607-D613 (2019).
411 21. Goncalves, R., Zhang, X., Cohen, H., Debrabant, A. & Mosser, D.M. Platelet activation attracts
412 a subpopulation of effector monocytes to sites of Leishmania major infection. *J Exp Med*
413 **208**, 1253-1265 (2011).

414 22. Leon, B., Lopez-Bravo, M. & Ardavin, C. Monocyte-derived dendritic cells formed at the
415 infection site control the induction of protective T helper 1 responses against Leishmania.
416 *Immunity* **26**, 519-531 (2007).
417 23. Ives, A.*, et al.* Leishmania RNA virus controls the severity of mucocutaneous leishmaniasis.
418 *Science* **331**, 775-778 (2011).
419 24. Novais, F.O.*, et al.* Genomic profiling of human Leishmania braziliensis lesions identifies
420 transcriptional modules associated with cutaneous immunopathology. *J Invest Dermatol*
421 **135**, 94-101 (2015).
422 25. Santos Cda, S.*, et al.* CD8(+) granzyme B(+)-mediated tissue injury vs. CD4(+)IFNgamma(+)-
423 mediated parasite killing in human cutaneous leishmaniasis. *J Invest Dermatol* **133**, 1533-
424 1540 (2013).
425 26. Boussoffara, T.*, et al.* Activated cytotoxic T cells within zoonotic cutaneous leishmaniasis
426 lesions. *Immun Inflamm Dis* **7**, 95-104 (2019).
427 27. Beechem, J.M. High-Plex Spatially Resolved RNA and Protein Detection Using Digital Spatial
428 Profiling: A Technology Designed for Immuno-oncology Biomarker Discovery and
429 Translational Research. *Methods Mol Biol* **2055**, 563-583 (2020).
430 28. Powles, T.*, et al.* MPDL3280A (anti-PD-L1) treatment leads to clinical activity in metastatic
431 bladder cancer. *Nature* **515**, 558-562 (2014).
432 29. Igarashi, T., Teramoto, K., Ishida, M., Hanaoka, J. & Daigo, Y. Scoring of PD-L1 expression
433 intensity on pulmonary adenocarcinomas and the correlations with clinicopathological
434 factors. *ESMO Open* **1**, e000083 (2016).
435 30. Roy, S., Saha, S., Gupta, P., Ukil, A. & Das, P.K. Crosstalk of PD-1 signaling with the
436 SIRT1/FOXO-1 axis during the progression of visceral leishmaniasis. *J Cell Sci* **132**(2019).
437 31. Donovan, M.J.*, et al.* Indoleamine 2,3-dioxygenase (IDO) induced by Leishmania infection of
438 human dendritic cells. *Parasite Immunol* **34**, 464-472 (2012).
439 32. Wang, F.*, et al.* RNAscope: a novel in situ RNA analysis platform for formalin-fixed, paraffin-
440 embedded tissues. *J Mol Diagn* **14**, 22-29 (2012).
441 33. Pardoll, D.M. The blockade of immune checkpoints in cancer immunotherapy. *Nat Rev*
442 *Cancer* **12**, 252-264 (2012).
443 34. Liu, M.*, et al.* Targeting the IDO1 pathway in cancer: from bench to bedside. *J Hematol Oncol*
444 **11**, 100 (2018).
445 35. Sharpe, A.H. & Pauken, K.E. The diverse functions of the PD1 inhibitory pathway. *Nat Rev*
446 *Immunol* **18**, 153-167 (2018).
447 36. Soliman, H.H.*, et al.* A phase I study of indoximod in patients with advanced malignancies.
448 *Oncotarget* **7**, 22928-22938 (2016).
449 37. Rosenberg, J.E.*, et al.* Atezolizumab in patients with locally advanced and metastatic
450 urothelial carcinoma who have progressed following treatment with platinum-based
451 chemotherapy: a single-arm, multicentre, phase 2 trial. *Lancet* **387**, 1909-1920 (2016).
452 38. Powles, T.*, et al.* Efficacy and Safety of Durvalumab in Locally Advanced or Metastatic
453 Urothelial Carcinoma: Updated Results From a Phase 1/2 Open-label Study. *JAMA Oncol* **3**,
454 e172411 (2017).
455 39. Heery, C.R.*, et al.* Avelumab for metastatic or locally advanced previously treated solid
456 tumours (JAVELIN Solid Tumor): a phase 1a, multicohort, dose-escalation trial. *Lancet Oncol*
457 **18**, 587-598 (2017).
458 40. Xu, J.-M.*, et al.* Phase I study of KN035, the first subcutaneously administered, novel fusion
459 anti-PD-L1 antibody in patients with advanced solid tumors in China. *Journal of Clinical*
460 *Oncology* **37**, 2608-2608 (2019).
461 41. Akinleye, A. & Rasool, Z. Immune checkpoint inhibitors of PD-L1 as cancer therapeutics.
462 *Journal of hematology & oncology* **12**, 92-92 (2019).

463 42. Joshi, T., Rodriguez, S., Perovic, V., Cockburn, I.A. & Stager, S. B7-H1 blockade increases
464 survival of dysfunctional CD8(+) T cells and confers protection against Leishmania donovani
465 infections. *PLoS Pathog* **5**, e1000431 (2009).
466 43. Makala, L.H.*, et al.* Leishmania major attenuates host immunity by stimulating local
467 indoleamine 2,3-dioxygenase expression. *J Infect Dis* **203**, 715-725 (2011).
468 44. Alessandra M. da Fonseca-Martins, T.D.R., Juliana E.S. Pratti, Luan Firmino-Cruz, Daniel
469 Claudio Oliveira Gomes, Lynn Soong, Elvira M. Saraiva, Herbert L. de Matos Guedes,.
470 Protection induced by anti-PD-1 and anti-PD-L1 treatment in Leishmania amazonensis-
471 infected BALB/c mice. *bioRxiv* (2019).
472 45. Liang, S.C.*, et al.* PD-L1 and PD-L2 have distinct roles in regulating host immunity to
473 cutaneous leishmaniasis. *Eur J Immunol* **36**, 58-64 (2006).
474 46. Kaye, P. & Scott, P. Leishmaniasis: complexity at the host-pathogen interface. *Nat Rev*
475 *Microbiol* **9**, 604-615 (2011).
476 47. Cassetta, L. & Pollard, J.W. Targeting macrophages: therapeutic approaches in cancer. *Nat*
477 *Rev Drug Discov* **17**, 887-904 (2018).
478 48. Ranawaka, R.R., Abeygunasekara, P.H. & Weerakoon, H.S. Correlation of clinical,
479 parasitological and histopathological diagnosis of cutaneous leishmaniasis in an endemic
480 region in Sri Lanka. *Ceylon Med J* **57**, 149-152 (2012).
481 49. Thilakarathne, I.K., Ratnayake, P., Vithanage, A. & Sugathadasa, D.P. Role of Histopathology
482 in the Diagnosis of Cutaneous Leishmaniasis: A Case-Control Study in Sri Lanka. *Am J*
483 *Dermatopathol* **41**, 566-570 (2019).
484 50. el Tai, N.O., Osman, O.F., el Fari, M., Presber, W. & Schonian, G. Genetic heterogeneity of
485 ribosomal internal transcribed spacer in clinical samples of Leishmania donovani spotted on
486 filter paper as revealed by single-strand conformation polymorphisms and sequencing. *Trans*
487 *R Soc Trop Med Hyg* **94**, 575-579 (2000).
488 51. Ranasinghe, S.*, et al.* Polymerase chain reaction detection of Leishmania DNA in skin biopsy
489 samples in Sri Lanka where the causative agent of cutaneous leishmaniasis is Leishmania
490 donovani. *Mem Inst Oswaldo Cruz* **110**, 1017-1023 (2015).
491 52. Goytain, A. & Ng, T. NanoString nCounter Technology: High-Throughput RNA Validation.
492 *Methods Mol Biol* **2079**, 125-139 (2020).

493

494 **Figure legends**

495 **Fig. 1. Differential expression and network analysis of genes regulated by drug**

496 **treatment a,** Volcano plot of differential expressed genes in patients on SSG treatment. A

497 fold change (FC) of 1.3 and a $p<0.05$ threshold were applied. Black dots indicate no

498 significance, red points indicate significant genes ($p< 0.05$), and blue points indicate

499 significantly altered genes that have a log2 (fold change) >1.3 **b,** List of top 14 genes that

500 changed expression in SSG treated patients. **c-d,** STRING protein-protein interaction

501 network[20](https://string-db.org) analysis was performed on genes listed in **Extended Data**

502 **Table 2** that changed as a consequence of two rounds of SSG treatment. Pathway analysis of

503 genes downregulated on treatment (**c**). Top 20 genes are shown (Log2fold change >1.25) for
504 clarity. Genes upregulated upon treatment are shown in (**d**)
505
506 **Fig. 2. Digital Spatial Profiling of CL lesions**
507 **a-f,** Regions of selection on sections from pre and on-treatment biopsies from patients P4, P6
508 and P7 (green: CD68 and red: CD3). ROIs were created on CD3 and/or $CD68^+$ rich areas. **g,**
509 List of all proteins used in the DSP panel and their significance scores when comparing
510 33ROIs at presentation and on treatment. Cells are highlighted in green to show decreasing
511 significance score from 0.055. Unpaired Students two-tailed t-test was applied to calculate
512 significance scores **h-j**, on-treatment ROIs have lower counts of IDO1 and PD-L1 but not
513 LAG3. Unpaired two-tailed Students t-test was applied to calculate significance scores. P-
514 values as indicated on graphs (n=33). **k-l**, Patients in validation cohort have lower IDO1 (**k)**
515 and PD-L1 (**l**) protein expression on treatment (n=25). Paired two-tailed Students t-test was
516 applied to calculate significance scores. p-values as indicated on graphs. Error bars represent
517 SD.
518
519 **Fig. 3 Immunofluorescence analyses of IDO1 in infected and uninfected cells**
520 **a,** Confocal image showing expression of IDO1 (red), CD68 (blue) proteins and *Amastin*
521 RNA probe. Both $IDO1^+CD68^+$ (arrow) and $IDO1^-CD68^+$ (arrowhead) cells are infected.
522 Scale bar, 10u. **b,** Representative scattergram (from patient P7 at presentation) colour coded
523 to show low, medium and high labelled IDO1 cells in cyan, red and green with respect to
524 *Amastin* dots. More *Amastin* dots containing cells correspond to medium and highly labelled
525 IDO1 cells. Each dot represents a single cell. **c-d,** Histograms showing fluorescence intensity
526 distributions of infected (**c**) and uninfected $IDO1^+$ cells (**d**). **e,** Representative violin plot
527 (from patient P7) showing significant reduction of mean fluorescent intensity of IDO1

528 labelled cells in *Amastin*- cells when compared to *Amastin*$^{+}$ cells. Dotted lines show median,
529 upper and lower quantile for each group. N=791 and 3872 for parasite positive and negative
530 cells, respectively. Significance score was generated using Students two tailed unpaired t-test.
531 P-value as indicated on the graph. **f,** Mean intensity of *Amastin*$^{+}$IDO1^{+} cells is significantly
532 higher than *Amastin*$^{-}$IDO1^{+} cells in all patients of test cohort, in which we could detect
533 parasites. Significance score was generated using Students two tailed paired t-test. P-value as
534 indicated on the graph.
535
536 **Fig. 4 Immunofluorescence analyses of PD-L1 in infected and uninfected cells**
537 **a,** A representative zoomed in confocal image showing protein expression of CD68, PD-L1
538 and *Amastin* RNA probe. Both PD-L1^{+}CD68^{+} (arrow) and PD-L1^{-}CD68^{+} (arrowhead) cells
539 are infected. Scale bar, 50 pixels **b,** Representative scattergram (from patient P24 at
540 presentation) showing *Amastin*$^{+}$ low (cyan), medium (red) and high (green) PD-L1
541 expressers with respect to *Amastin* dots. More *Amastin* dots containing cells correspond to
542 medium and highly labelled PD-L1 cells. **c-d,** Histograms showing fluorescence intensity
543 distributions of infected (**c**) and uninfected (**d**) PD-L1 cells. **e,** Representative violin plot
544 (from patient P24) showing significant reduction of mean fluorescent intensity of PD-L1
545 labelled cells in *Amastin*$^{-}$ cells when compared to *Amastin*$^{+}$ cells. Dotted lines show median,
546 upper and lower quantile for each group. N=9159 for parasite positive cells and 41520 for
547 parasite negative cells. Significance score was generated using Students two tailed unpaired t-
548 test. P-value as indicated on the graph. **f,** Mean intensity of *Amastin*$^{+}$PD-L1^{+} cells is
549 significantly higher than *Amastin*$^{-}$PD-L1^{+} cells in all patients (n=7). Significance score was
550 generated using Students two tailed paired t-test. P-value as indicated on the graph.
551
552

553

554 **Supplementary Figure Legends and Tables**

555 **Extended Data Fig. 1 CONSORT flow diagram** Flow chart shows number of patients who
556 were screened, treated, followed up in early assessment, completed the study and included in
557 the final analysis. For more details on the patients refer to Extended Data Table 1. PBMCs:
558 Peripheral Blood Mononuclear Cells; SSG: Sodium Stibogluconate; Cryo: Liquid nitrogen
559 cryotherapy.

560

561 **Extended Data Fig. 2 CL lesions from test cohort patients** Lesions in patients were
562 photographed at presentation and 3mm tissue biopsy were taken from the border of the
563 lesion. **a-l,** Lesion photographs from patients P1 (**a**), P4 (**b**), P5 (**c**), P6 (**d**), P7 (**e**) and -P8 (**f**)
564 at presentation**)** and during treatment (**g-l)**.

565

566 **Extended Data Fig. 3. Histopathology of test cohort**

567 **a-l**, Hematoxylin and eosin stains on whole 4u tissue sections and magnified areas from
568 patients P1 (**a**), P4 (**b**), P5 (**c**), P6 (**d**), P7 (**e**) and P8 (**f**) at presentation and on treatment **(g-l).**
569 Scale bar is 100u in whole sections and 20u in zoomed in areas.

570

571 **Extended Data Fig. 4 Heterogeneity of patient response to treatment**

572 **a,** For each patient, Pearsons correlation (r) was computed using R studio from 770 genes in
573 the nCounter PanCancer Immunology Panel codeset at presentation and on-treatment and
574 plotted as a heat map. While pre-treatment shows positive linear correlations, pre- and on-
575 treatment samples do not, indicating that despite a limited sample size, the data sets are
576 robust enough to reveal differences between matched pre- and on-treatment samples. On-

577 treatment samples are not as highly correlated amongst themselves as the pre-treatment
578 cohort suggesting a degree of heterogeneity in patient response to treatment.
579
580 **Extended Data Fig. 5: ROI strategy for DSP**
581 12 ROIs were generated in each pre-treatment and on-treatment section from each patient. **a,**
582 Representative images from patient P4 of each ROI selected from at presentation showing
583 ROI strategy. ROIs were created on both $CD3^+$ and/or $CD68^+$ immune infiltrates. **b-c,** Bar
584 graphs show housekeeping (HK) normalised CD68 (**b**) and CD3 (**c**) counts in each ROI. **d,**
585 Representative images from patient P4 of each ROI selected on-treatment. **e-f,** Bar graphs
586 show housekeeping (HK) normalised CD68 (**e**) and CD3 (**f**) counts in each ROI.
587
588 **Extended Data Fig. 6 Consort diagram of validation cohort patients**
589 Flow chart shows number of patients who were screened, treated, followed up in early
590 assessment, completed the study and included in the final analyses SSG: Sodium
591 Stibogluconate; Cryo: Liquid nitrogen cryotherapy
592
593 **Extended Data Fig. 7 Pateint photographs and histology of validation cohort**
594 **a-c,** Representative patient photograph at baseline (**a**) and showing improvement after 4
595 weeks (**b**) and 3 month (**c**). **d-e,** H & E staining on tissue biopsy sections taken at
596 presentation (**d**) and after 4 weeks of treatment (**e**).
597
598 **Extended Data Fig. 8 Gating strategy for low, medium and highly labelled IDO1 cells**
599 **a,** Grey image of zoomed in heterogenous IDO1 expression in skin tissue biopsy. **b**, $IDO1^+$
600 cells as detected using Strataquest image analysis software. **c-e,** Cells were binned based on
601 mean fluorescence intensities of each cell into high (**c**), moderate (**d**) and low (**e**) expression,

602 respectively. **f,** Representative histogram showing distribution of *Amastin* dots in IDO1$^+$
603 cells. *Amastin*$^+$ and *Amastin*$^-$ are defined by an *Amastin* count of 1, as shown by vertical bar.
604 Some data points are off scale **g-i,** Histograms (**g-h**) and violin plot (**i**) showing fluorescence
605 intensity distribution of *Amastin*$^+$IDO1$^+$ cells (**g, i**) and *Amastin*$^-$ IDO1$^+$ cells (**h, i**) in patient
606 P5 at presentation. N=7404 and 16610 for parasite positive and negative cells, respectively.
607 **j-l,** Histograms (**j-k**) and violin plot (**l**) showing fluorescence intensity distribution of
608 *Amastin*$^+$IDO1$^+$ cells (**j**) and *Amastin*$^-$ IDO1$^+$ cells (**k**) in patient P8. N=672 and 2758 for
609 parasite positive and negative cells, respectively Significance score was generated using
610 Students two-tailed, unpaired t-test. P-value as indicated on the graph.
611
612 **Extended Data Fig 9. Co-expression of IDO1/PD-L1 and CD68**
613 **a-b,** Representative confocal image of a pre-treatment section showing infection in
614 (*Amastin*$^+$, green) IDO1$^+$ (red) CD68$^-$ (blue) cells. Scale bar, 50 pixels **b**, Trend line graph
615 from patients P4-P8 showing changes in number of IDO1$^+$CD68$^-$ cells with treatment. Each
616 dot represents average of 2 biological replicates for each patient. *p = 0.0481, Two tailed,
617 Paired Student's t test. (**c**) Representative zoomed in confocal image of a pre-treatment
618 section showing co-expression of PD-L1 and CD68. *Amastin*$^+$ parasites are shown in green.
619 Scale bar, 50 pixels.
620
621 **Extended Data Fig 10 Gating strategy for low, medium and high PD-L1 expressing cells**
622 **a,** Grey image of zoomed in heterogenous PD-L1 expression in skin tissue biopsy. **b,** PD-L1$^+$
623 cells as detected using Strataquest image analysis software **c-e,** Cells were binned based on
624 mean fluorescence intensities of each cell into high (**c**), moderate (**d**) and low (**e**) expression,
625 respectively. **f,** Representative histogram showing distribution of *Amastin* dots in PD-L1$^+$
626 cells. Axis scale was adjusted to demonstrate the cut off (1 *Amastin* dot) used for PD-L1$^+$

627 cells containing *Amastin* dots. Some data points are off scale. **g-l,** Scattergram from *Amastin*$^+$
628 at presentation sections from P9 (**g**), P13 (**h**), P16 (**i**), P17 (**j**), P23 (**k**) and P29 (**l**)
629 respectively, showing higher number of *Amastin* dots in medium (red) and high (dark yellow)
630 PD-L1 expressers than those cells showing low expression of PD-L1 (cyan).
631
632 **Extended Data Fig 11 Infected PD-L1$^+$ cells have greater fluorescence intensity than**
633 **uninfected PD-L1$^+$ cells**
634 **a-f,** Histograms and violin plots showing fluorescence intensity distributions of all infected
635 and uninfected PDL1 cells of P9 (**a**), P13 (**b**), P16 (**c**), P17 (**d**), P23 (**e**) and P29 (**f**) at
636 presentation respectively. Dotted lines show median, upper and lower quantile for each
637 group. N>240 and >9000 were analysed for parasite positive and negative cells respectively
638 from each patient.
639
640 **Extended Data Fig 12 Model for SSG-T cell synergy during CL treatment**
641 Lesions in patients with readily detectable numbers of viable parasites have higher expression
642 of PD-L1 and IDO1 at presentation contributing to T cell exhaustion (Tex; top most panel).
643 Within 2-4 weeks of treatment, SSG-dependent reduction in amastigote load facilitates
644 decreased expression of PD-L1 and IDO1 by intralesional CD68$^+$ cells, helping to restore
645 effector T cell (Teff) function and synergy with SSG. Whether restored T cell function alone
646 would be sufficient to clear residual parasite burden and accomplish re-epithelialization
647 remains to be tested.
648
649 **Extended Data Table 1 Demographics of patients in test cohort**
650
651 **Extended Data Table 2 Details of total DE genes on treatment**

652

653 **Extended Data Table 3 Log2 (fold change) and adjusted p-value of DE transcripts of**

654 **common regulators/effectors of human leishmaniasis analysed in this study.**

655

656 **Extended Data Table 4 Demographics of patients in validation cohort**

657

658

a

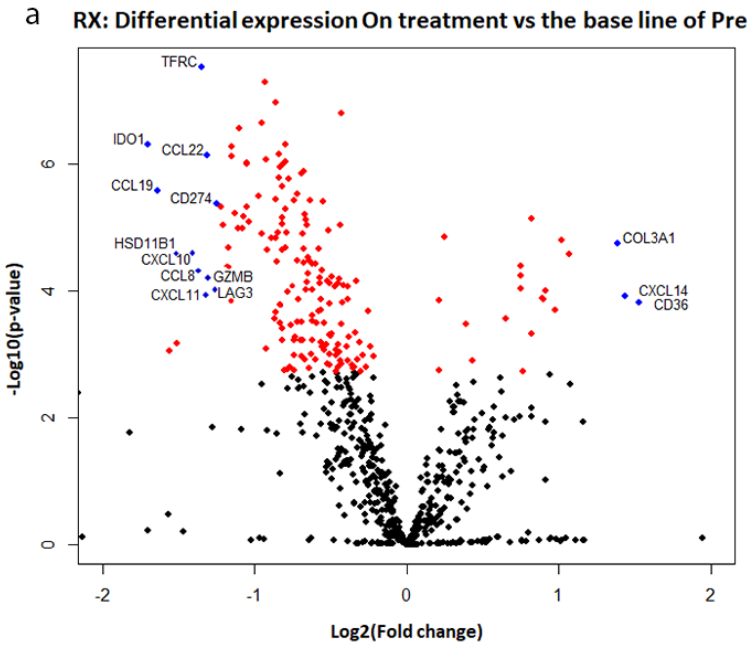

b

	Log2 fold change	P-value	adjusted P-value	Gene.sets
IDO1	-1.7	4.96E-07	0.00029	Cytokines, T-Cell Functions
CCL19	-1.64	2.64E-06	0.000542	Chemokines, Regulation
HSD11B1	-1.52	2.45E-05	0.00189	Cell Functions
CXCL10	-1.4	2.77E-05	0.00207	Chemokines, Cytokines, Pathogen Defense, Regulation, T-Cell Functions
CCL8	-1.37	4.97E-05	0.00319	Chemokines, Regulation
TFRC	-1.35	2.94E-08	0.000124	T cell regulation
CXCL11	-1.32	0.00011	0.00543	Chemokines, NK Cell Functions, T-Cell Functions
CCL22	-1.31	7.31E-07	0.00029	Chemokines, Pathogen Defense
GZMB	-1.3	6.26E-05	0.00377	Cell Functions, Cytotoxicity
LAG3	-1.28	9.92E-05	0.005	Regulation, T-Cell Functions
CD274	-1.25	4.15E-06	0.000661	B-Cell Functions, Cell Functions, T-Cell Functions
COL3A1	1.39	1.80E-05	0.00155	Regulation
CXCL14	1.44	0.000122	0.00594	Chemokines
CD36	1.53	0.000152	0.00688	Transporter Functions

c

Genes down-regulated on treatment
(Adjusted p-value<0.01; Log2Fold change>1.25)

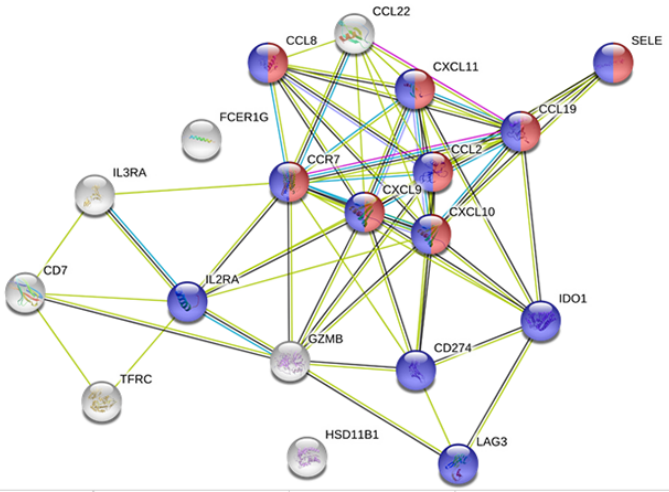

pathway ID	*pathway description*	*count in gene set*	*false discovery rate*
GO:0002687	positive regulation of leukocyte migration	8	6.33E-11
GO:0002684	positive regulation of immune system process	12	8.55E-10

d

Genes up-regulated on treatment
(Adjusted p-value<0.01; Log2Fold change>0.8)

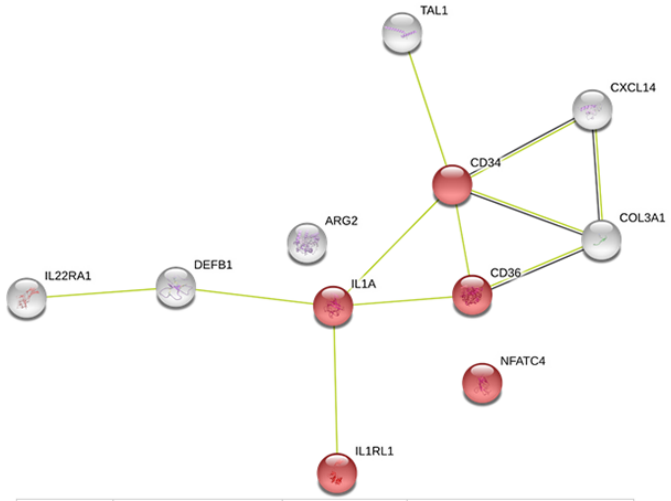

pathway ID	*pathway description*	*count in gene set*	*false discovery rate*
GO:0001819	positive regulation of cytokine production	5	0.006

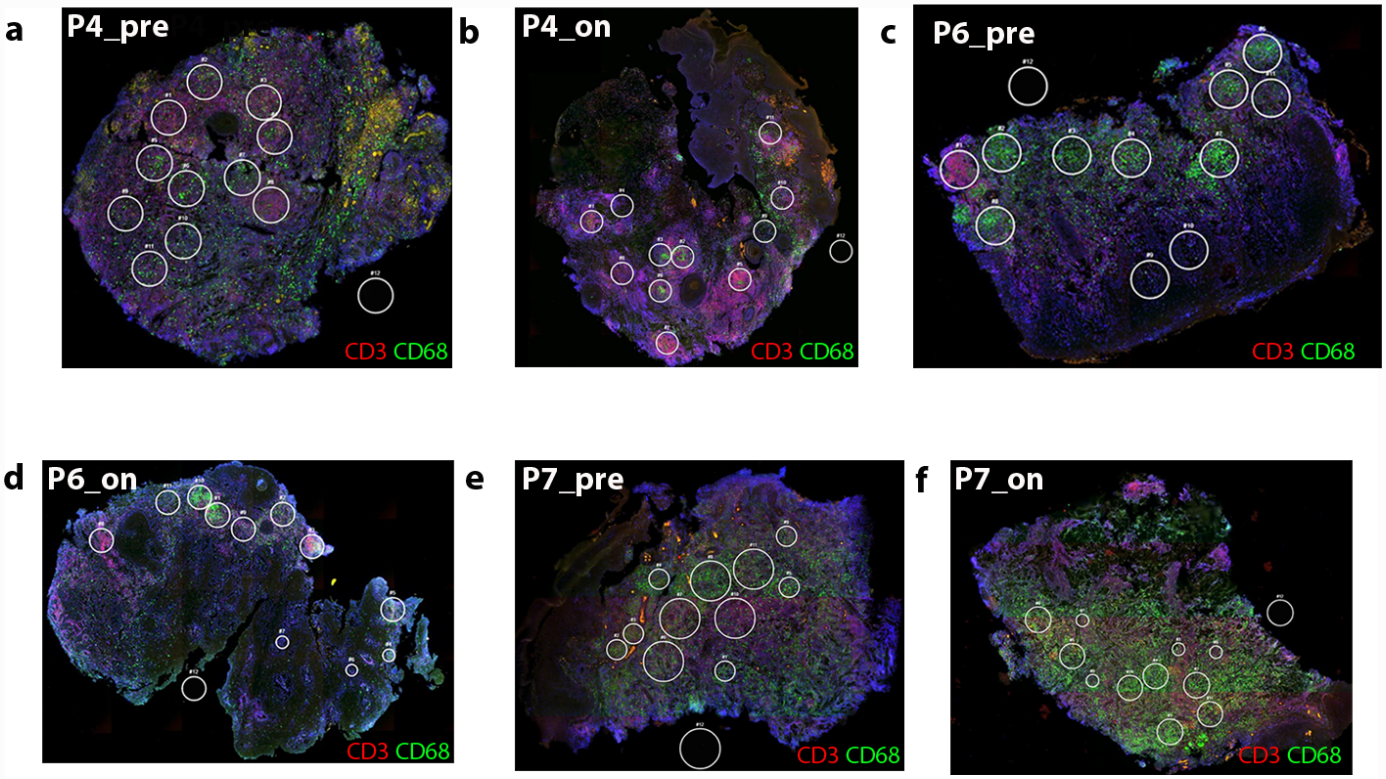

g Rx: Significant scores of differentially expressed proteins On-treatment vs Pre

Proteins	p-value	Proteins	p-value	Proteins	p-value
CD40L	1.0	TGFB1	0.4	CD45	0.043
ER alpha	1.0	NY-ESO-1	0.3	PD-L2	0.028
PanCk	1.0	LAG3	0.3	CD45RO	0.026
CD20	1.0	MART1	0.3	PD-L1	0.020
S100B	0.9	FOXP3	0.3	ARG1	0.020
B7-H3	0.8	4-1BB CD137	0.2	ICOS	0.019
CD56	0.8	PD-1	0.2	CD25	0.014
CD27	0.8	CD163	0.2	CD44	0.013
PR	0.7	Rb IgG	0.2	STING	0.010
Ms IgG1	0.6	FAPalpha	0.2	VISTA	0.010
EpCAM	0.6	CD8	0.2	IDO1	0.0094
SMA	0.6	CD68	0.2	CD40	0.0089
Ms IgG2a	0.5	OX40L	0.1	HLA-DR	0.0028
S6	0.5	GAPDH	0.1	CD86	0.0024
CTLA4	0.5	CD80	0.1	CD14	0.0012
GITR	0.5	PTEN	0.099	CD66b	0.0011
Histone H3	0.4	Bcl-2	0.071	Tim-3	0.00029
Fibronectin	0.4	Beta-2-microglobulin	0.070	GZMB	0.00007
CD11c	0.4	CD4	0.055	Ki-67	0.00006
Her2/ErbB2	0.4	CD34	0.047		
CD127	0.4	CD3	0.047		

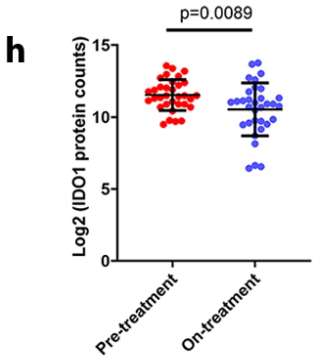

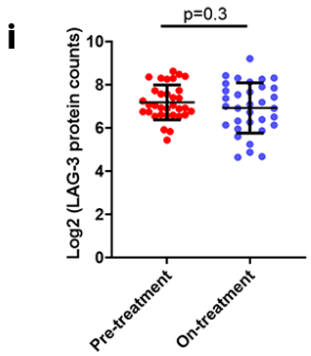

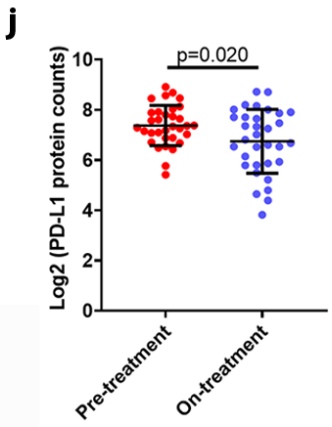

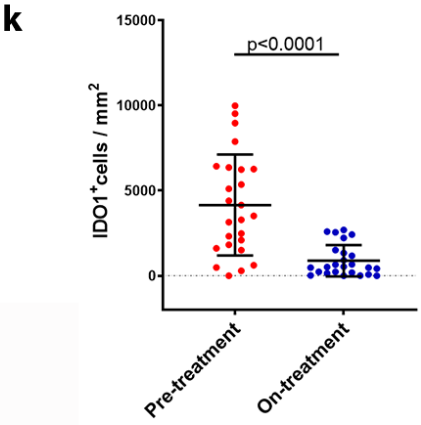

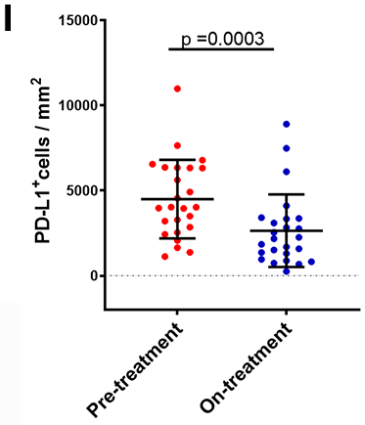

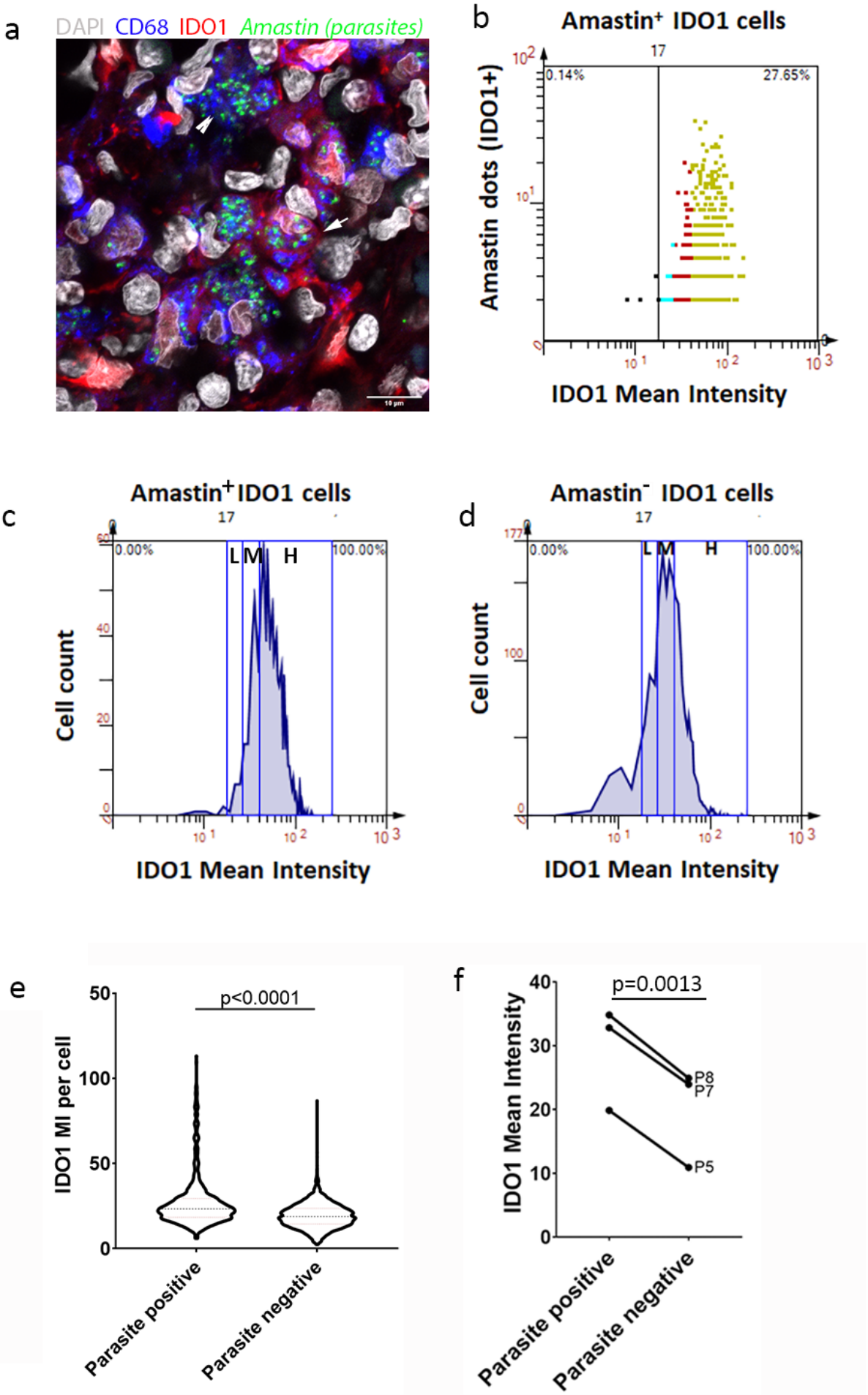
a
DAPI CD68 IDO1 Amastin (parasites)
b
Amastin+ IDO1 cells
17
0.14%
27.65%
Amastin dots (IDO1+)
IDO1 Mean Intensity
c
Amastin+ IDO1 cells
17
0.00%
L M H
100.00%
Cell count
IDO1 Mean Intensity
d
Amastin- IDO1 cells
17
0.00%
L M H
100.00%
Cell count
IDO1 Mean Intensity
e
p<0.0001
IDO1 MI per cell
Parasite positive
Parasite negative
f
p=0.0013
IDO1 Mean Intensity
P8
P7
P5
Parasite positive
Parasite negative

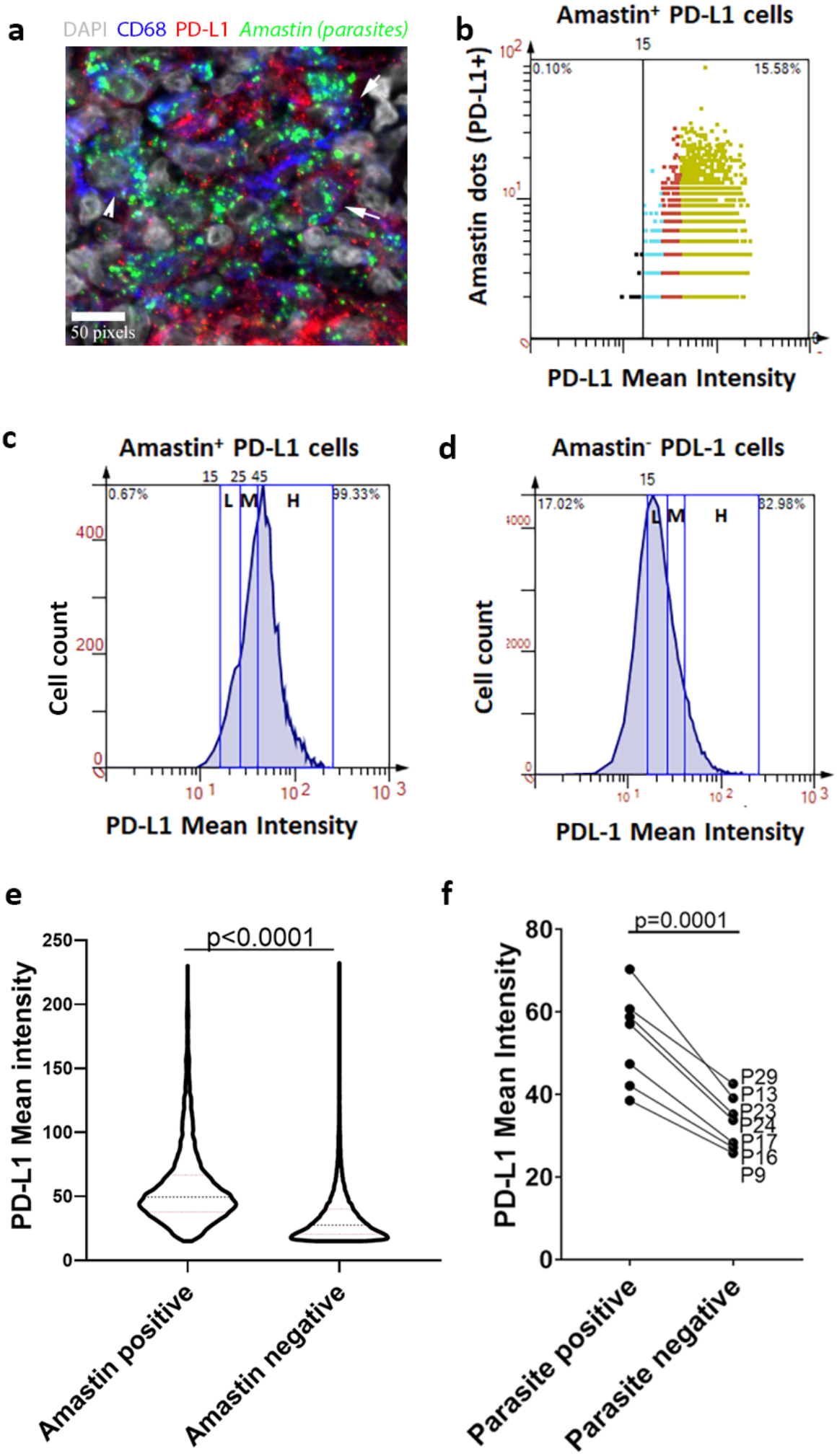
a
DAPI CD68 PD-L1 Amastin (parasites)
50 pixels
b
Amastin+ PD-L1 cells
Amastin dots (PD-L1+)
PD-L1 Mean Intensity
0.10%
15.58%
15
c
Amastin+ PD-L1 cells
Cell count
PD-L1 Mean Intensity
0.67%
99.33%
L
M
H
15
25
45
d
Amastin- PDL-1 cells
Cell count
PDL-1 Mean Intensity
17.02%
82.98%
L
M
H
15
e
PD-L1 Mean intensity
p<0.0001
Amastin positive
Amastin negative
f
PD-L1 Mean Intensity
p=0.0001
P29
P13
P23
P24
P17
P16
P9
Parasite positive
Parasite negative